Title:

Long-lasting event-related beta synchronization and theta desynchronization of electroencephalographic activity in response to support-surface perturbations during upright stance: Novel findings from experimental and model-based results

Authors:

Akihiro Nakamura, Yasuyuki Suzuki, Matija Milosevic, and Taishin Nomura

Affiliation:

Division of Mechanical Science and Bioengineering, Graduate School of Engineering Science,
Osaka University, Osaka, Japan

Corresponding Author:

Taishin Nomura, Ph.D.
Division of Mechanical Science and Bioengineering,
Graduate School of Engineering Science,
Osaka University, Osaka, Japan
Email: taishin@bpe.es.osaka-u.ac.jp

Running Title:

Long-lasting beta ERS and theta ERD during perturbed upright stance

Number of figures: 5
Number of tables: 0
Abstract word count: 299 words

Keywords: upright posture, postural control, electroencephalogram (EEG), event-related synchronization (ERS), beta rebound

Abstract

Movement related beta band cortical oscillations, including post-movement beta rebound and desynchronization/synchronization observed during Go/NoGo tasks, have drawn attention in motor control literature, particularly during movements of upper extremities. However, fewer study focused on beta band oscillations during postural control in upright stance. Here, we examined beta rebound and other components of electroencephalogram (EEG) activity during perturbed upright stance to investigate supraspinal contributions to postural stabilization. Particularly, we aimed to clarify the timing and duration of the beta rebound and other components within a non-sustained, but long-lasting, postural recovery process following perturbed stance that occurs much more slowly compared to upper extremities due to a larger time scale of mechanical dynamics. To this end, EEG signals were acquired from nine healthy young adults in response to an impulsive support-surface perturbation, together with the center of pressure (CoP), center of mass (CoM) and electromyogram (EMG) activities of ankle muscles. Event-related potentials (ERPs) and event-related spectral perturbations (ERSPs) were computed using the perturbation onset as a triggering event. Our results indicate that, after short-latency (<0.3 s) ERPs, powers in high-beta and alpha bands decreased (event-related desynchronizations: ERDs) in the 0.3-0.6 s and 0.3-1.5 s time-intervals after the perturbation onset, respectively. This was followed by long-lasting theta band decrease (ERD) and high-beta increase (event-related synchronization: ERS), implying beta rebound. Specifically, the beta rebound sustained for approximately three seconds from 1.0 to 4.0 s. EMGs of the ankle muscles and joint torques of the ankle and hip were almost completely relaxed in the first half period of the beta rebound. In the remaining period, the CoP and CoM were in their final approach to the equilibrium with amplitudes comparable to those during quiet stance. Possible mechanisms of beta rebound and long-lasting theta-ERD may be related to underlying intermittent control strategy for upright stance.

Introduction

Supraspinal contributions to postural stabilization during human upright stance have been evidenced by postural instability in patients with neurological disorders such as Parkinson's disease (PD), multiple sclerosis, and stroke (Frzovic et al. 2000; Geurts et al. 2005; Horak et al. 1992; Perera et al. 2018; Visser et al. 2008; Yamamoto et al. 2011). Alterations in patterns of postural sway and postural responses to perturbations induced by a cognitive load (Woollacott and Shumway-Cook 2002) and by motor learning during adapting to novel environmental demands (Horak and Nashner 1986) also provide a glimpse into the roles played by the supraspinal networks in the control of upright posture.

Measuring electroencephalogram (EEG) activity and/or motoneuronal responses to transcranial magnetic stimulation (TMS) during standing are more direct ways to characterize electrical activity of the cerebral cortex associated with postural control. For example, using EEG recordings, it has been clarified that postural reactions against mechanical perturbations during voluntary postural sway are triggered by the central command mechanisms associated with bursts of gamma-band activities (Slobounov et al. 2005). Soleus muscle showed larger motor evoked potentials in response to TMS stimuli during standing on a moving planform compared to standing on a still platform, implying increased cortico-spinal excitability in more challenging postural environments (Solopova et al. 2003). Yet, there is very limited knowledge of how activities of the cerebral cortex, particularly those measured by EEG, encode sensory information processing and motor control during stabilization of upright stance (Bolton 2015; Jacobs and Horak 2007; Wittenberg et al. 2017).

EEG signals during upright stance have been investigated traditionally using event-related potentials (ERPs) in response to postural brief perturbations, where a perturbation-event-locked average of EEG

signals is computed to achieve high signal-to-noise ratios. Particularly, the most representative ERP, referred to as the N1 with a negative potential, has been identified in EEG activities in response to brief mechanical perturbations (Quant et al. 2005; Varghese et al. 2017). The N1 potential is induced typically with a latency of about 90-170 ms and amplitude ranging from -10 to -70 μV, with responses spatially distributed over frontal, central, and parietal cortices (Varghese et al. 2017). There are two interpretations for the origins of the N1 responses. One considers that N1 represents a neural processing of sensory information necessary for coordinating reactive balance responses based on the fact that the latency and amplitude of N1 are altered depending on the afferent transmission delay and the level of cognitive load, respectively (Dietz et al. 1984, 1985; Dimitrov et al. 1996; Quant et al. 2004; Staines et al. 2001). Another interpretation is that N1 represents an error signal for detecting postural instability (Adkin et al. 2006, 2008; Mochizuki et al. 2009). Moreover, Payne *et al*. showed that N1 includes startle responses not only balance-correcting motor responses (Payne et al. 2018). In a recent review article by the same group, it was suggested that N1 and error-related negativity reflect similar function (Payne et al. 2019). Similarly, they showed N2 is not evoked in PD patients (Payne and Ting 2020). Taken together these studies provide insights into specific cortical responses to balance perturbations during upright stance, which are affected in PD patients.

Time-frequency characteristics of EEG responses induced by mechanical perturbations can be summarized into event-related spectral perturbations (ERSPs) (Mierau et al. 2017; Slobounov et al. 2005; Solis-Escalante et al. 2019; Varghese et al. 2014, 2015), in which neural oscillations at distinct frequency-bands represent the balance of neuronal excitation and inhibition (Buzsáki et al. 2012; Muthukumaraswamy 2014). Using EEG ERSPs, it may be possible to identify cortical responses to particular events during standing as shown for other motor and cognitive tasks (Makeig 1993; Pfurtscheller and Lopes da Silva 1999). For motor tasks other than the upright posture, it is considered

that low-frequency band-limited cortical synchronizations (< 20 Hz) are associated with a deactivated state of the corresponding networks, and high-frequency band-limited cortical synchronizations (>20 Hz) reflect a state of active information processing (Pfurtscheller and Lopes da Silva 1999). Particularly, event-related desynchronizations (ERDs) at beta band (13-30 Hz) prior to and/or during motor execution as well as event-related synchronizations (ERSs) of beta band oscillations after the movement are well known (Pfurtscheller et al. 1996; Pfurtscheller and Lopes da Silva 1999). The beta band ERS is typically referred to as the post-movement rebound or simply as beta rebound, and it is considered to be associated with *status quo* in terms of the postural maintenance of upper extremities (Engel and Fries 2010) and afferent sensory information processing (Cassim et al. 2001). Attenuation of the beta rebound in PD patients reported by Vinding *et al*. is consistent with impaired sensory integration in the PD patients (Vinding et al. 2019). Moreover, the beta rebound observed in Go/NoGo tasks, with and without motor executions, is also a typical research paradigm in movement-related EEG responses (Alegre et al. 2004; Swann et al. 2009; Zhang et al. 2008). Since the ERS for the NoGo response is not accompanied with an actual motor execution, it may represent not only information processing of sensory feedback signals, but also motor-related decision-making processes in the supraspinal networks. Together with attenuated ERS responses reported for the Go/NoGo task in PD patients (Wu et al. 2019), it may be considered that the beta ERD and beta rebound represent information processing performed by the cortico-basal ganglia motor loop.

Among a small handful of studies analyzing ERSPs during upright stance, Mierau *et al*. reported that whole-body perturbations during upright stance increases EEG powers in theta (3-7 Hz), alpha (8-12 Hz), and beta bands, within very short latencies of the response (at most few hundred ms), corresponding to the time range of the N1 potentials (Mierau et al. 2017). However, beta rebound, which has been examined extensively during voluntary and passive motor tasks in upper extremities,

has not been reported for the postural control tasks during upright stance. One of the key issues in dealing with postural recovery processes during upright standing in response to external perturbations is the difference in the time-scale of mechanical dynamics compared to movements of the upper extremities. Namely, motor responses of the central nervous system during upright stance typically persist over longer time periods (i.e., a few seconds), unlike those of the upper extremities that are typically completed within a few hundred milliseconds.

In this study, we examined ERSPs during the long-lasting postural recovery process to the upright equilibrium state in response to small impulsive (step-like) support-surface perturbations. A particular interest was to investigate the timing and the duration of beta band ERD and ERS responses, and characterized them quantitatively. Because a postural recovery process from a perturbed posture to the upright equilibrium is transient, and it settles down eventually to the post-recovery upright equilibrium state, this could be regarded as a *status quo* for a postural maintenance. Therefore, similar to the upper limbs (Engel and Fries 2010), we could expect that beta ERD and subsequent post-movement beta rebound (ERS) to present in the EEG cortical activities following upright stance perturbations, as well as other ERS and ERD responses, although movements considered in the upper-limb studies are often self-initiated, which would involve distinct cortical control including anticipation. If we could observe beta ERD and a beta rebound as hypothesized, the main scientific novelty to clarify in the current study would be related to characterizing the temporal profiles of the appearance of the beta activities within the long-lasting postural response in the musculo-skeletal system. In the simplest possible situation, a beta ERD would appear persistently during a slow postural response during muscular activities, and then a beta rebound would appear following postural recovery, i.e., after upright posture is fully recovered within the long-latency duration of about a few seconds. This hypothesized mechanism is the exact same process of beta band ERD and ERS during upper extremity motor tasks

(Engel and Fries 2010). However, variations of possible time intervals allotted for ERD and ERS timing may be expected due to the long-lasting postural response. These novel temporal characterizations of the beta band ERD and ERS accompanied with the slow musculoskeletal dynamics would provide a crucial perspective on the mechanistic interpretation of the beta ERD as well as the beta rebound during upright stance.

Methods

Participants

Nine healthy young male participants (mean age 24.2 years, SD 1.4 years) were included in the study. None of the participants suffered from neurological disorders nor used medications that could influence movement. All participants gave written informed consent. The study was executed in accordance to the Declaration of Helsinki (2013) and was approved by the ethical committee of the Graduate School of Engineering Science at Osaka University.

Experimental protocol

Standing posture, electromyography (EMG) and EEG signals were measured under the following two conditions: quiet standing (control) and support-surface perturbation (perturbed). Postural sway during quiet stance in the control condition was measured to determine the equilibrium posture and to distinguish a transient postural recovery from the equilibrium state. In each trial with either control or perturbed condition, participants were asked to stand still for 7 min on a treadmill (Bertec, Ohio, USA) with their arms folded on the chest, while fixing their gaze straight ahead at a target located in the longitudinal direction of the treadmill belt at the same height as their eyes. That is, the anterior-posterior (AP) direction of postural sway was set parallel to the longitudinal direction of the treadmill belt. The participants performed two trials for each condition, thus, four trials in total. The order of

four trials with two conditions were randomized for each participant. A sufficient rest of at least 3 min was given between trials. The support-surface perturbation was applied during upright stance by moving the treadmill-belt backward slightly and quickly using an in-house computer-program. Each perturbation spanned 200 ms, which was composed of an acceleration phase (4 m/s^2 for 100 ms), followed by a deceleration phase (-4 m/s^2 for 100 ms). The perturbation was applied 20 times with a fixed interval of 20 s. The participants could keep upright stance easily against each perturbation without having to initiate compensatory stepping or other overt movements in any of the trails. We confirmed that no participants could make an accurate prediction to brace for the perturbation, based on an oral questionnaire at the end of the experiment. The participants were instructed to stand upright in a relaxed state to reduce the effects of muscle-activity-derived artifacts in EEG recordings, which could be induced by eye-movements and/or eye-blinking.

Experimental setup

Postural kinematics were measured using a 3-dimensional optical motion capture system (SMART-DX, BTS Bioengineering, Milan, Italy) with a sampling frequency of 300 Hz, where light reflection markers were attached on the left and right ankles, greater trochanters, and acromions. The AP and medio-lateral (ML) changes in posture were quantified by measuring the center of pressure (CoP), in which a force plate built in the treadmill acquired time-profiles of the ground reaction force vectors at a sampling frequency of 1200 Hz. EMG signals were recorded from the ankle muscles of left and right legs, including soleus (SO), medial-gastrocnemius (MG) and tibialis anterior (TA), using wireless surface electromyograms (FreeEMG, BTS Bioengineering, Milan, Italy) with a sampling frequency of 1 kHz. EEG signals were measured using a 32 electrodes mobile bio-amplifier and a shielded waveguard cap with active shielded cables for reducing movement-induced interference (eegosports, ANT Neuro, Hengelo, Netherlands). Specifically, Ag/AgCl electrodes were arranged in accordance to

the International 10/10 system (Chatrian et al. 1985; Jurcak et al. 2007). All electrodes used CPz as a reference, and one frontal electrode was used as ground (GND). The impedance at all electrodes was controlled to be less than 20 kΩ during the measurements (Ferree et al. 2001). Cortical EEG oscillation signals were sampled at a sampling frequency of 2,048 Hz.

Analysis of CoP during quiet stance

Postural sway data during quiet stance (control condition) in each participant were characterized using CoP time-series. In short, the standard deviations of CoP variations, slopes of linear regression lines for the log-log plotted power spectrum of CoP in AP direction at low (0.02-0.2 Hz) and high (1-8 Hz) frequency regimes were calculated, as described elsewhere (Matsuda et al. 2016; Yamamoto et al. 2011, 2015).

Joint angles and CoM analysis

Human body during upright stance was modeled using a triple-inverted pendulum of rigid links, with the head-arm-trunk (HAT) link, a leg-link, and a foot-link, moving in the sagittal plane around two pinned-joints corresponding to the ankle and hip joints (Suzuki et al. 2012). The foot-link was assumed to be fixed on the support-surface. The ankle joint angle θ_{a} was defined as the tilt angle of the leg-link from the vertical upward line, and the hip joint angle θ_{h} was defined as the relative joint angle between the HAT- and the leg-links. The joint angles were estimated from the marker positions for each participant. Specifically, positions of two markers on the left and right sides of the body were projected on the sagittal plane, and they were averaged to obtain the position data for each of the ankle (x_{ANK}, y_{ANK}), greater trochanter (x_{GT}, y_{GT}), and acromion (x_{AC}, y_{AC}). Then, θ_{a} and θ_{h} were defined as follows.

$$\theta_{\mathrm{a}} = -\arctan((x_{\mathrm{ANK}} - x_{\mathrm{GT}})/(y_{\mathrm{ANK}} - \mathrm{y}_{\mathrm{GT}})),$$

$$\theta_{\mathrm{h}} = -\arctan((x_{\mathrm{GT}} - x_{\mathrm{AC}})/(y_{\mathrm{GT}} - \mathrm{y}_{\mathrm{AC}})) - \theta_{\mathrm{a}},$$

for which the counterclockwise rotation (plantar flexion for the ankle joint and extension for the hip joint) was defined as the positive direction. For full details related to the model, see Appendix A.

Horizontal position of the total body center of mass (CoM) in the AP direction during standing was estimated as

$$CoM = \frac{m_{\mathrm{L}} x_{\mathrm{L}} + m_{\mathrm{HAT}} x_{\mathrm{HAT}}}{m_{\mathrm{L}} + m_{\mathrm{HAT}}}, \tag{1}$$

$$x_{\mathrm{L}} = \left(\frac{l_{\mathrm{L}}}{2}\right) \sin \theta_{\mathrm{a}}, \tag{2}$$

$$x_{\mathrm{HAT}} = l_{\mathrm{L}} \sin \theta_{\mathrm{a}} + \left(\frac{l_{\mathrm{HAT}}}{2}\right) \sin(\theta_{\mathrm{a}} + \theta_{\mathrm{h}}), \tag{3}$$

where l_{HAT} representing the HAT-length is determined by the mean distances between (x_{GT}, y_{GT}) and (x_{AC}, y_{AC}) and l_{L} representing the leg-length is determined by the mean distances between (x_{ANK}, y_{ANK}) and (x_{GT}, y_{GT}) for each participant. m_{HAT} and m_{L} are the masses of the corresponding links, estimated from the total body weight of each participant using a statistical formula of $m_{\mathrm{HAT}}{:}\, m_{\mathrm{L}} = 0.62{:}\ 0.35$ (Suzuki et al. 2012). We assumed that the CoM of each link was located at the middle point of the link. CoM time-series were smoothed by a zero-lag fourth-order Butterworth filter with a cutoff frequency of 10 Hz. CoM velocity time-series were calculated using the central difference of the filtered CoM data.

Event-locked average

For the perturbed condition, postural responses with respect to the perturbation onset were characterized by event-locked average profiles of the ankle and hip joint angles, the position and velocity of CoM and CoP for each participant, as well as for averaged profiles across participants, where the onset of each perturbation was used as a triggering event. That is, time-series data recorded

for each trial were segmented into a number of small pieces of the data, referred to as epochs, each of which corresponds to a single perturbation, and the event-locked average time-profile was obtained by calculating the mean of the segmented data over the epochs for each participant. The event-locked average joint angles, CoM and CoP profiles were compared with the corresponding time-profiles of event-locked average responses of EMGs, ERPs and ERSPs. For our analysis, each joint angle, joint torque, CoM, CoP, EMG time-profile was plotted after subtracting its mean to adjust the baseline representing the equilibrium point of each variable. Peaks of the event-locked average responses were detected, for which latencies from the triggering event was obtained.

CoP analysis

In the perturbed condition, the foot position shifted backward in response to every perturbation by the amount of the backward shift of the belt. Because the force plate and its local coordinate system were fixed in the world coordinate system independent of the moving belt, a time-profile of the recorded CoP position during the 7 min, which is denoted by $x_{\mathrm{cop}}^{\mathrm{W}}(t)$ in the world coordinate system as a function of time t, was the sum of a time-profile of the actual postural response $x_{\mathrm{cop}}(t)$ and a series of step-wise backward shifts of the belt that was measured as the position of the ankle joint $x_{\mathrm{ANK}}(t)$ both in the world coordinate system, i.e., $x_{\mathrm{cop}}^{\mathrm{W}}(t) = x_{\mathrm{cop}}(t) + x_{\mathrm{ANK}}(t)$. In this way, we obtained the CoP time-series as $x_{\mathrm{cop}}(t) = x_{\mathrm{cop}}^{\mathrm{W}}(t) - x_{\mathrm{ANK}}(t)$, which represents the actual postural response to the perturbation. The CoP time-series was then low-pass filtered offline using the zero-lag fourth-order Butterworth filter with a cutoff frequency of 10 Hz, while the CoP velocity time-series was obtained using the central differences of the filtered CoP data. The event-locked average CoP response (averaged across participants) was plotted as a function of time. Moreover, CoP and CoM trajectories were plotted on the CoP/CoM-position v.s. CoP/CoM-velocity plane as a phase plane (Asai et al. 2009).

Joint torque estimation

Joint torques exerted on the ankle τ_{a} and the hip τ_{h} as the sum of passive and active torques during postural recovery responses were estimated by solving inverse dynamics based on the triple-inverted pendulum model, the motion captured body kinematics (θ_{a}, θ_{h} and CoM), the CoP positions, and the ground reaction force vectors. For full details related torque estimation, see Appendix B.

EMG analysis

The EMG data recorded from MG, SO and TA were processed with a zero-lag 20-450 Hz band-pass fourth-order Butterworth filter, full-wave rectified, and then low-pass filtered using a zero-lag second-order Butterworth filter with a cutoff frequency of 15 Hz (Merletti and Di Torino 1999; Winter et al. 1980; Yoshida et al. 2017). Because we were particularly interested in the postural dynamics in the AP-direction, processed EMGs from the left and right legs for each muscle were averaged, which was defined as integrated EMGs (iEMGs) of the corresponding muscle for each participant. Then, an event-locked average of iEMG for each participant was normalized by its maximum value using the peak iEMG profile for each participant. The normalized event-locked average of iEMGs were used to analyze peak latency and peak height for each muscle.

EEG analysis

Preprocessing, denoising, and analysis of EEG signals were conducted using EEGLAB (Delorme and Makeig 2004; Loo et al. 2019). First, EEG data were down-sampled to 1 kHz to reduce the computational time required for further processing. A zero-lag high-pass first-order Butterworth filter with a cutoff frequency of 1 Hz was applied to optimize signal-to-noise ratio (Winkler et al. 2015). We then removed data from noisy electrodes because we used the average reference potential method (Bigdely-Shamlo et al. 2015), for which a large noise in one electrode would affect the other electrodes.

In this study, an electrode was considered as large noise if the correlation coefficients between the surrounding electrodes were smaller than 0.8. The average number of electrodes rejected in single trials was 0.28.

We performed the artifact subspace reconstruction (ASR), which is a method for denoising EEG signals using principal component analysis (PCA) (Mullen et al. 2015). Steps of the ASR processing are summarized as follows: (1) Find and extract time less noisy intervals from the 32-dimenional EEG time-series and apply PCA to the extracted data to define the template dataset which represents the EEG signal basis vectors of the principal components (i.e., principal axes); (2) Decompose all EEG time-series data within a time-window of 1.0 s into the principal axes to obtain the magnitude of variance for each principal axis; (3) Remove components if their variances were 20 times larger compared to those of the corresponding components in the template data, and reconstruct the EEG for this window using other remaining components; and (4) Repeat the decomposition while shifting the time-window with 66% overlap (Mullen et al. 2015). After ASR, data for the removed electrodes were spatially and linearly interpolated using the data from the surrounding electrodes. Finally, re-referencing was performed based on the average potential of all the electrodes by which tendencies for the electrodes around CPz which are smaller in their amplitude were eliminated.

To remove eye-blinking and muscle-activity from the EEG data, independent component analysis (ICA) was performed. Artifact components were defined using the method described by Bruijn et al. (2015). That is, if the average power in the frequency band between 50 to 100 Hz of the IC was larger compared to the average power of alpha band (8 to 12 Hz) or low-beta band (13 to 20 Hz), these components were considered to originate from muscle activity. For each IC, if its central frequency was under 3 Hz and its topographic-map-representation was distributed around the forehead, this IC

was considered to originate from eye-blinking, i.e., electrooculograms (EOGs). In a single trial, the mean number of removed EMG components was 2.3, and the mean number of removed EOG components was 1.6. After removing those artifact ICs, the remaining ICs were re-mapped onto the electrodes. The re-mapped EEG data in the time interval from 5 s before the perturbation until 10 s after the perturbation was then used as an epoch.

ERP was calculated for each electrode by computing the event-locked average over all epochs (Davis et al. 1939; Quant et al. 2005). For quantifying ERP of each electrode, the largest and the second largest peak amplitudes in positive and negative directions for the ERP time-profile were detected for each participant, where the peaks could either be positive or negative. Those peaks were expected to correspond to P1, N1, P2, and N2 potentials (Quant et al. 2005). Moreover, ERPs were plotted on the scalp as a function of time (as snapshots) to characterize spatio-temporal distribution of the ERP responses.

Outcomes of time-frequency analysis for each epoch for each electrode were summarized by averaging them over epochs over all perturbations, for each participant and across participants to obtain ERSPs (Makeig 1993). For each epoch, we performed a time-frequency analysis using the wavelet transform with the Morlet wavelet ψ(t) defined as

$$\psi(t) = \frac{1}{\sqrt{2\pi\sigma^2}} e^{-\frac{t^2}{2\sigma^2}} e^{j2\pi t},$$

where the number of cycles for the continuous wavelet transformation that defines σ was increased gradually from 3 to 24 corresponding to the range of 3 to 60 Hz, which covers all relevant EEG frequency bands: theta (3-7 Hz); alpha (8-13 Hz); low-beta (13-20 Hz); high-beta (20-30 Hz); and gamma (40-60 Hz). An outcome of ERSP was presented by plotting wavelet coefficients as a function of time (*t*) and frequency (*f*) on the time-frequency plane. Moreover, we plotted the temporal change

(snapshot) of the spatial distribution of power on the scalp using the average amplitude for each frequency band.

For a given ERSP on the time-frequency plane, clustered regions with enhanced and attenuated spectral powers were identified, corresponding to ERS and ERD, respectively. We examined appearances of ERS and ERD for every frequency band, and quantified a time-profile of spectral power at the corresponding band. To this end, power values at each time instant were summed up over the corresponding frequency band. For each identified ERS/ERD, latency of the peak of the cluster were characterized.

Because prominent ERS and ERD were identified at high-beta and theta bands, which were expected to sustain for relatively long periods as shown later, time-duration of the high-beta ERS (beta rebound) and theta ERD were quantified. Time-duration of each cluster (ERS/ERD) was characterized as follows: time axis in the time-frequency plane between -2.5 to 8 s with the perturbation-onset being at the origin was divided into bins with time-width of 0.5 s and frequency-height of 10 Hz between 20 and 30 Hz for high-beta band, moreover with the time-width of 0.5 s and frequency-height of 3 Hz between 4 and 7 Hz for theta band. The mean power was then averaged over the time and frequency within each of the 21 bins (21 discretized latencies) that were computed for each participant. In this way, participant-wise nine coarse-grained-series of high-beta-band powers and those of theta-band powers were obtained. Amplitude and latencies of each ERD/ERS were analyzed for each participant (participant-wise average) and then across participants to characterize average time-profiles.

Statistical analysis

Statistical comparisons of the time-duration of the high-beta ERS (beta rebound) and the theta ERD

in ERSP were examined using multiple comparison tests for their coarse-grained-series. To this end, a distribution of mean values across participants was examined for each discretized latency, where normality of the distribution of mean values was examined by the Lilliefors test (Lilliefors 1967). The bin for the latency between -2.5 and -2 s was selected to represent the resting power level, which was well prior to the perturbation. The mean power of this bin was compared with that of each of the remaining bins at different latencies using the Dunnett's test (Dunnett 1955, 1964) to examine whether the power at each latency was significantly different compared to the resting power. The level of statistical significance was set at 0.05 for all tests. All statistical comparisons were performed using MTALB (Mathworks, USA).

Results

CoP during quiet stance

Postural sway during quiet stance (control condition) for can be summarized as follows. Standard deviation of sway in the AP direction was about 10 mm on average, which was approximately two times larger than that in the ML direction. Specifically, the average CoP sway distance in AP direction was 10.6 ± 4.9 mm and ML direction was 6.4 ± 3.8 mm. The slope of the linear regression line for the log-log plotted power spectrum of CoP in the AP direction at the high frequency regime was -2.85 ± 0.48, and that at the low frequency regime was -1.68 ± 0.35. In particular, the power spectrum in the low frequency regime exhibited the $f^{-\beta}$-type scaling with the exponent close to $\beta = 1.5$, as predicted by the intermittent postural control hypothesis (Asai et al. 2009; Collins and De Luca 1994; Nomura et al. 2013).

Responses to the perturbation

Fig. 1 shows the event-locked average responses to the support-surface perturbations averaged across participants for the joint angles in panel A and torques in panel B for the ankle and hip joints, the positions of CoM and CoP in panel C, and CoP−CoM (i.e., the position of CoP relative to that of CoM) in panel D, which should be approximately proportional to the ankle joint torque in the perspective of the single-inverted pendulum model, EMGs of SO and MG in panel E and their magnifications in panel F, EMG of TA in panel G and its magnification in panel H, ERP for Cz-electrode in the identical panels of panel I and J, and ERSP for Cz also in the identical panels of K and L.

Kinematic and kinetic responses to the perturbation

During the support-surface acceleration for $0 < t < 100$ ms, the leg-link tilted forward (i.e., the proximal end of the leg-link) moved forward) due to the sudden backward shift of the feet (i.e., the distal end of the leg-link) as confirmed by the changes in θ_{a} in negative/dorsiflexion direction in Fig. 1A. The forward shift of the proximal end of the leg-link induced a forward shift in the distal end of the HAT-link, resulted in the backward tilt of the HAT-link relative to the leg-link (i.e., changes in θ_{h} toward positive/extension direction in Fig. 1A). Because $|\theta_{\mathrm{a}}| \simeq \theta_{\mathrm{h}}$ on this occasion, the tilt of the HAT-link in the world coordinate system was maintained around the upright position, i.e., $\theta_a + \theta_{\mathrm{h}} \simeq 0$. Moreover, the anti-phase movement of the ankle and hip joint angles at the initial phase of the postural response curbed the forward shift of CoM below 0.01 m as confirmed in Fig. 1C at the approximate time of 100 ms.

During the support-surface deceleration for $100 < t < 200$ ms, inertia forces pulled the body backward to oppose the acceleration period. However, they were not large enough to reverse the movement directions of θ_{a} and θ_{h}, and thus, the leg-link continued tilting forward, and the HAT-link continued

rotating backward relative to the leg-link as shown in Fig. 1A at $100 < t < 200$ ms.

In the middle of the acceleration period ($t \sim 60$ ms), SO and MG activities were initiated, and peaked at $t \sim 150$ ms in the middle of deceleration period (Fig. 1E). Those muscle activities generated plantar-flexion torque at the ankle to brake the forward tilt (Fig. 1B with the upward plantar-flexion peak of the ankle joint torque at $t \sim 210$ ms), leading to the changes in θ_{a} in the negative/dorsiflexion direction of the leg-link, which reversed the rotation direction of θ_{a} at the downward dorsiflexion peak at $t \sim 200$ ms in Fig. 1A.

The direction reversal in the leg-link (θ_{a}) toward the upright position at $t \sim 200$ ms initiated the backward shift of the distal end of the HAT-link, which induced the reversal in θ_{h} to the negative/flexion direction (the upward peak of the hip joint extension at t ~ 200 ms in Fig. 1A). A contribution of the hip joint torque for this direction reversal was small, as confirmed by the small hip joint torque at $t \sim 200$ ms in Fig. 1B.

Up to this point, and for another few hundred milliseconds, the extension of θ_{h} and the dorsiflexion of θ_{a} varied in an anti-phasic manner with similar amplitudes, leading to $\theta_{\mathrm{a}} + \theta_{\mathrm{h}} \simeq 0$. Thus, the forward shift of HAT, determined by Eq. (3), could be simply regarded as $l_{\mathrm{L}} \sin \theta_{\mathrm{a}}$, and together with Eqs. (1) and (2), the forward position of CoM was determined solely by θ_{a}. In this way, the downward dorsiflexion peak of θ_{a} coincided with the peak of the CoM forward-shift at $t \sim 200$ ms in Fig. 1C. The CoP continued to move forward after the CoM peak, and peaked at $t \sim 300$ ms. The difference between CoP and CoM (CoP−CoM) showed a qualitative agreement with the ankle joint torque (compare Figs. 1B and D).

After the dorsiflexion peak, θ_a decayed monotonously, and almost recovered the equilibrium at $t \sim$ 1000 ms. The corresponding ankle joint torque decayed almost to zero at $t \sim 2000$ ms. The hip joint angle θ_h decreased in the negative/flexion direction until it reached the downward hip-flexion peak at $t \sim 500$ ms, reversed again to the positive/extension direction (Fig. 1A). In contract to the hip-extension peak, the direction reversal at the hip-flexion peak was induced by the hip joint torque peaked at $t \sim 330$ ms in Fig. 1B. After the hip-flexion peak, θ_h and the hip joint torque decayed monotonously to the equilibrium within the interval of $t \in [2000, 3000]$ ms.

Phase plane trajectories

Fig. 2 shows the event-locked average of CoP/CoM profiles (averaged across participants) in the CoP/CoM-position v.s. the CoP/CoM-velocity phase plane. The left panel spans the range of whole response that exhibited a perturbation-induced large excursion, whereas the right panel spans a range of postural sway during quiet stance to display the CoP/CoM responses at the very latest phase of the postural recovery. Note that the vertical dashed line in the right panel indicates the standard deviation of the postural sway during the quiet standing. The small circles with blue, red and black colors plotted on the CoM trajectory in the left and/or right panels indicate the time instants of 0.5, 1.0 and 2.0 s, respectively. The triangles with the same colors indicate the corresponding time instants on the CoP trajectory. Both of CoM and CoP trajectories after $t = 1.0$ s (the red circles and triangles) approached the equilibrium posture at the origin in a linear manner (i.e., each of CoP and CoM trajectories shaped like a line) with no oscillations around the origin, as if the inverted-pendulum system were overdamped. The trajectories after $t = 2.0$ s (the black circles and triangles) were very close to the equilibrium, but still along the above-mentioned lines, meaning that the postural state did not move randomly even within this small region near the origin, but the postural recovery dynamics in this last phase still possessed strong deterministic structure that did not vanish by the event-locked averaging.

EEG responses revealed by ERP and ERSP

Fig. 1-I (and the panel J, which is exactly the same as the panel I) represents the ERP time-profile (averaged across participants) for Cz-electrode located on the primary motor area. Figure 1K (and the panel L, which is exactly the same as the panel K) represents the ERSP (averaged across participants) also for Cz-electrode. In Fig. 3, the spatial distributions of ERP (top trace) and ERSP for five frequency-bands are plotted on the scalp as snapshots at 15 latencies from -500 to 4000 ms.

As in the previous study (Quant et al. 2005), the ERPs of P1, N1, P2 and N2 were confirmed around the Cz-electrode (Fig. 1I and J and 3-top). Those ERP potentials could be decomposed into ERSs at the frequency-bands of gamma, low-beta, alpha and theta that appeared all together within the initial phase before $t \sim 300$ ms after the perturbation-onset (Fig. 1K and Fig. 3).

Latency and peak amplitude of the P1 potential was 41 ± 18 ms and 5.1 ± 2.3 μV, respectively, which was immediate before the onset of SO, MG and TA activations. The P1 was mainly composed of ERSs at frequency-bands of low-beta and alpha, each of which was spatially localized around Cz-electrode (Fig. 3 at 40 ms).

Latency and peak amplitude of the N1 potential was 116 ± 22 ms and -17.2 ± 6.2 μV, respectively, which was immediate after the onset of support-surface deceleration, and followed a few tens of milliseconds by the peaks of SO, MG and TA activities. The N1 was composed of the low-beta ERS peaked at 94 ± 20 ms for Cz, alpha ERS peaked at 92 ± 26 ms for Cz, and theta ERS peaked at 124 ± 30 ms for Cz with a minor contribution of the gamma ERS (Figs. 1K and L), where the low-beta ERS and alpha ERS for N1 were part of (i.e., continuation of) the corresponding ERSs that contributes to

P1. Note that the high-beta-ERS showed almost no contribution to P1 and N1 potentials. The low-beta ERS and theta ERS (and also the gamma ERS) for N1 were spatially distributed over the scalp, but the alpha ERS was localized around Cz-electrode (Fig. 3).

Latency and peak amplitude of the P2 potential was 264 ± 49 ms and 8.5 ± 3.6 μV, respectively, which was a few tens of milliseconds after the termination of the support-surface deceleration, immediate after the end of large activations of SO, MG, middle of the large TA activation, and well corresponded to the peak of forward-shift of CoP (Fig. 1C), consistent with a previous study (Slobounov et al. 2005). Moreover, it coincided in time with the largest peak of the hip extension torque (Fig. 1B). P2 was mainly composed of the gamma ERS peaked at 252 ± 106 ms for Cz (Figs. 1K and L). Note that there was one outlier with a very large latency of the gamma-band ERS, which was removed for computing the mean latency. The gamma ERS for P2 was spatially distributed over the scalp. Although P1 and P2 might also have contributions from the theta ERS distributed over the scalp, the appearance of the theta ERS for P1 and P2 was likely due to the low resolution (the uncertainty principle) of the wavelet at the low-frequency band.

During the postural recovery in the range from 300-600 ms, ERD at high-beta band (high-beta ERD) was observed dominantly at Cz (Figs. 1K and L) and weakly at C_3 and C_4 (Fig. 3). The peak latency of the high-beta ERD was 450 ± 83 ms for Cz, which was roughly coincided with the N2 potential (Figs. 1K and L). Moreover, it also coincided with the time instant when the CoP on the way back to the upright position caught and surpassed the CoM that preceded the CoP until that point (Fig. 1C), altering the sign of CoP−CoM from positive with a momentum forcing the CoM backward for recovering the forward-tilted posture to negative with a momentum forcing the CoM forward for braking the backward-moving posture (Fig. 1D). Those momenta were mostly generated by body

mechanics induced by the relative positioning between CoP and CoM, which could be confirmed by the fact that the large EMG responses of SO, MG and TA were already in the late of their decreasing phases. However, those muscle activities also contributed to the stabilization (Figs. 1F and H). In this way, the high-beta ERD did not necessarily appear in the middle of the large EMG responses, but it appeared at the end of the large responses of SO and MG. Since the large activation of TA was delayed relative to those of SO and MG (about 50 ms difference in the peak latencies) and also it decayed more slowly than SO and MG, the high-beta ERD overlapped with the late phase of the large TA activation.

For latencies longer than 1.0 s, we found two event-related clusters of powers in ERSP (Figs. 1K and L). One was the ERS at high-beta band (high-beta ERS), which appeared after the high-beta ERD. The high-beta ERS lasted for a long duration with its peak latency located at 3.27 ± 1.35 s. The high-beta ERS was observed mainly at Cz-electrode (Fig. 3). Fig. 4 shows time evolution of the high-beta ERS. Distributions of the powers of high-beta band at discretized boxes were normal, except the bins at [-0.5 0] s and [-5.5 6.5] s. The averaged powers across participants at the high-beta band at Cz-electrode in the latency between 1 and 4 s, for about 3 s, were significantly greater than the resting potential ($p < 0.05$, Dunnett's test). During the appearance of the high-beta-ERS, the CoP and the CoM became close to each other in the very late phase of the recovery process (Figs. 1A and C). This could also be confirmed by Fig. 2 that shows the trajectories of postural response (averaged across all subjects) in the CoP/CoM-CoP/CoM velocity phase plane. Particularly, the trajectories within the period of time when the high-beta-ERS was significantly large is indicated by the red curve segments in the phase plane of Fig. 2, by which we could observe that the postural state during the appearance of the high-beta ERS was located in the area very close to the range of postural sway during quiet stance. However, as mentioned above, the postural state during the high-beta ERS did not move randomly, but still it moved mostly deterministically along the above-mentioned lines. Comparison between ERSP in Fig.

1L and enlarged EMGs in Figs. 1F and H showed that activations of SO and MG muscles were slightly larger than those during quiet stance for the early period ($1 < t < 3$ s) of the high-beta-ERS. However, activations of all muscles were almost the same as those during quiet stance for the later phase ($3 < t < 4$ s) of the high-beta-ERS. That is, the high-beta-ERS in its later phase was generated with almost no perturbation-induced muscular activations.

In addition to the high-beta-ERD, ERD at alpha and theta bands were also observed. As shown in Fig. 3, the alpha ERD appeared at the occipital region for the early phase ($t \sim 270$ ms), and then expanded to the whole head, with the latency 0.83 ± 0.17 s at Cz. The time interval of the alpha ERD coincided with the period of time when the sign of CoP−CoM was negative with a momentum forcing CoM forward for braking the backward-moving posture (Fig. 1D). Then, the theta-ERD appeared specifically around Cz with its latency of 1.88 ± 0.74 s. Fig. 4-right quantifies the time-range of the theta-ERD. Distributions of the powers of theta band at discretized boxes were normal, except the boxes at [1.5 2] s and [3.5 4] s. The averaged powers across participants at the theta-beta band at Cz-electrode in the latency box of [1, 1.5] s was significantly smaller than the resting potential ($p < 0.05$, Dunnett's test). Although no statistical significance was obtained, the theta-ERD also exhibited a long-lasting property as in the high-beta-ERS, which could be visually confirmed in Figs. 1K and L that the blue-colored ERD at theta band until the latency of 3.0 s.

Discussion

In this study, we examined the postural recovery process during upright stance in response to the support-surface impulsive perturbation. Slower time-scale of mechanical dynamics during postural perturbations compared to movement of the upper extremities, prompted analysis of the temporal profile of cortical activations during postural stabilizing process. It was shown that neural responses

for re-stabilizing upright posture lasted over a relatively long period of time (i.e., few seconds), unlike those of the upper extremities, which typically last few hundred milliseconds (Engel and Fries 2010; Pfurtscheller et al. 1996; Pfurtscheller and Lopes da Silva 1999). During the initial phase of the postural recovery process which was within a few hundred milliseconds, we confirmed P1, N1, P2, and N2 peaks of the event-related potentials (ERPs), consistent with a previous study (Quant et al. 2005). For the longer time scale after the initial phase, we found event-related synchronizations (ERSs) and desynchronizations (ERDs) during postural recovery toward the upright stance, unlike that observed in upper extremity responses. Particularly, we identified a novel type of ERS at high-beta band (high-beta ERS or beta rebound) localized around Cz-electrode over the primary motor area, which occurred with a long latency from the perturbation-onset ($t \sim 1.0$ s) and was long-lasting for about 3 s (Fig. 1K and Fig. 3).

Reflexive responses in the initial phase

ERSs that we observed other than the high-beta ERS were at the gamma frequency-band, low-beta, alpha and theta that appeared all together within the initial phase of the response (within about 300 ms after the perturbation-onset) as shown in Fig. 1K and Fig. 3. Specifically, the P1 potential (with the peak latency of 40 ms) was composed of the low-beta and alpha ERSs that were located at Cz-electrode, and occurred immediate before the onset of SO, MG and TA activations. The very short latency of P1 (slightly less than 50 ms) is similar to that of vestibular-evoked potential (Todd et al. 2014), which might trigger centrally the initial muscular responses.

Additional recruitment of the ERS components mainly at the theta band developed the P1 potential into the N1 potential (with the peak latency of 120 ms as reported in the previous studies (Mierau et al. 2017; Slobounov et al. 2005)). It has been considered that N1 represents a neural processing of

sensory information necessary for coordinating reactive balance responses (Dietz et al. 1984, 1985; Dimitrov et al. 1996; Quant et al. 2004; Staines et al. 2001). Moreover, it might represent an error signal for detecting postural instability (Adkin et al. 2006, 2008; Mochizuki et al. 2009). Those sensory information processing might contribute to enhancing the muscle activations of SO and MG that were initiated by the spinal stretch reflexes, because the N1 potential was followed by the large activations of SO and MG. Moreover, the large response of TA muscle peaked at 200 ms, which overrode a possible action of reciprocal inhibition from the SO/MG activations, might be mainly excited centrally by the N1 potential to stiffen the ankle joint by counteracting to the SO/MG-induced plantar-flexion ankle torque peaked at 150 ms.

The P2 potential was dominantly composed of the gamma ERS, which might represent a neural detection of postural instability (Slobounov et al. 2005). It was followed by the largest peak of hip extension torque, implying that the P2 potential might be associated with the generation of extension torque at the hip joint (Figs. 1B and K). Further examinations with EMGs of hip joint muscles are required for validating the active contribution of the P2 to the control of hip joint movement.

ERD at high-beta band at the end of the initial phase

In this study, the ERD at high-beta band (high-beta ERD) was observed dominantly around the primary motor area. It peaked at 450 ms, roughly coincided with the N2 potential. In general, (high-)beta ERDs have been identified for motor tasks other than the upright stance, in which they appear at the beginning of (or sometimes slightly prior to) the movement and sustain during the movements (Jurkiewicz et al. 2006; Neuper and Pfurtscheller 1996; Pfurtscheller et al. 1996; Pfurtscheller and Lopes da Silva 1999). A recent study suggested that a smooth execution of a voluntary movement requires a decrease in the power of beta band (Heinrichs-Graham and Wilson 2016), suggesting that

beta ERDs in general are associated with the preparation of actions and related information processing to facilitate a motor execution. Note that beta ERDs appear even in passive (non-voluntary) motor tasks (Vinding et al. 2019) and also in Go/NoGo tasks regardless of the motor selection (Go or NoGo response) (Alegre et al. 2004; Wu et al. 2019). That is, beta ERDs are not necessarily accompanied with actual motor executions, but they, together with beta ERSs, represent an information processing of afferent sensory signals as well as the decision-making process (Jurkiewicz et al. 2006, Alegre et al. 2004; Wu et al. 2019). The high-beta ERD in this study appeared when the CoP recovering toward the upright position caught and surpassed the CoM, after which CoP and CoM began to be close to each other. It also coincided with the period of time when the muscle activations became much smaller than those in the initial phase of the postural response for $t < 300$ ms. This seemingly contradicts with a typical way of the appearance of beta ERDs, because the high-beta ERD in this study was not accompanied with the major muscle activations for $t < 300$ ms. However, the major muscle activations with the large postural response for $t < 300$ ms could be considered as a stereo-typical sequence of reflexes both at spinal and cortical levels, and the postural control after the initial phase might require a sophisticated information processing to achieve the postural recovery, which might be represented in the high-beta ERD in this study. For example, the high-beta ERD after the initial postural response could represent a state of preparing for possible actions after the perturbation, such as a stepping response in case that the perturbation is larger than a threshold, by inhibiting the reflexive muscular reactions during the initial phase of the postural response and by facilitating the cortico-spinal excitability (Solopova et al. 2003). Those interpretations are consistent with the recent report on N2 potential reflecting specific cortical responses to balance perturbations during upright stance, which are affected in PD patients (Payne and Ting 2020).

ERD at alpha and theta bands

At the later phase of the high-beta ERD, the alpha ERD appeared at the occipital region for the early phase ($t \sim 270$ ms), which might correspond to the previously reported ERD at mu band (Jurkiewicz et al. 2006), and then expanded to the whole head until about $t \sim 1$ s (Fig. 3). Then, the theta ERD appeared specifically around Cz with its latency of $t \sim 800$ ms lasting for about 1 s (Fig. 4-right). During the time interval with the alpha ERD and theta ERD, the CoM was located close to or slightly ahead of the CoP, while the body was recovering toward the upright position. Although no statistical significance was obtained, the theta ERD exhibited a long-lasting property as in the high-beta ERS until the latency of 3.0 s. The appearance of movement-related theta ERD is completely novel, to our best knowledge, and thus we avoid interpreting it. However, because it sustained for a long period together with the beta rebound, it might play a complementary role in the sensory information processing.

The long-lasting ERS at high-beta band

A (high-)beta ERS, also known as beta rebound, appears typically after the completion of a movement, and often following the corresponding beta ERD (Jurkiewicz et al. 2006; Neuper and Pfurtscheller 1996; Pfurtscheller et al. 1996; Pfurtscheller and Lopes da Silva 1999). The high-beta ERS identified in this study appeared also after the high-beta ERD. However, it began before the postural recovery was completed (Figs. 1A and K), which is different from previous studies for the upper extremities. A simple interpretation that accounts for the difference is to consider that the major response was completed within the initial phase of the recovery process, and the small residual postural response remained during the beta ERS would be negligible. If this is the case, we could consider that the high-beta ERS in this study was also initiated after the movement as in the previous studies for the upper extremities, implying the same functional roles expressed by the high-beta ERS in this study as others

in the previous studies for the upper extremities. That is, the cortical beta activity in humans represents a raise in the activity levels that penalize voluntary movement (Gilbertson et al. 2005; Pastötter et al. 2008; van Wijk et al. 2009), while actively promoting postural maintenance (Gilbertson et al. 2005). The promotion of postural maintenance may be achieved through an up-regulation of relevant sensory inputs during and immediately after bursts of beta activity (Androulidakis et al. 2006; Gilbertson et al. 2005; Lalo et al. 2008). Indeed, beta ERS power during finger movement is reduced in patients with impaired afferent sensory information processing due to Parkinson's disease (PD) (Vinding et al. 2019). Moreover, ischemia in the peripheral afferent reduces the power of beta rebound (Cassim et al. 2001). However, beta ERS does not simply represent the postural maintenance, but the postural maintenance that demands certain amounts of information processing, which is suggested by the reduction of beta-ERS power during visually cued isometric hand grips (Rossiter et al. 2014). As in the beta ERD, the beta ERS appears not only after actual motor execution, but also after a motor imagery and/or after NoGo response in Go/NoGo task (Pfurtscheller and Lopes da Silva 1999; Wu et al. 2019). Moreover, the beta ERS power in PD patients is attenuated (Wu et al. 2019). Those evidences suggest that the beta-ERS represents a processing of afferent sensory information (Jurkiewicz et al. 2006) and a decision-making process (Alegre et al. 2004; Wu et al. 2019) in combination with the beta ERD.

Novel interpretation of the long-lasting beta rebound

An alternative interpretation is required if the small residual postural dynamics remained during the beta ERS would not be negligible, which might be supported by the fact that the CoP/CoM state points during the beta ERS still exhibited strong deterministic structure that did not vanish through the event-locked averaging (Fig. 2-right). In this case, we should conclude that the beta ERS appeared before the perturbation-induced movement was completed, which would be a novel process to have beta rebound activities. Moreover, the high-beta ERS sustained for about 3 s is also a novel property that

has not been observed so far. In the above-discussed interpretation of the beta ERS, we considered that the small residual error remained would be negligible, based on which the end of the major postural response during the initial phase would correspond to the terminal of the perturbation-induced movement, triggering the post-movement high-beta ERS. However, if this is the case, such negligibly small postural response could not be a cause of the long-lasting high-beta ERS, and the high-beta ERS should have completed in a shorter duration than three seconds. Thus, it turns out that small residual postural dynamics converging to the upright equilibrium might not be simply "almost equilibrated state," but they should still be taken care of for accomplishing the postural stabilization, which requires a certain amount of information processing of afferent sensory signals and decision-making, leading to the long-lasting high-beta ERS.

We speculate that the long-lasting high-beta ERS at the late phase of postural recovery might be associated with the recently proposed intermittent control during human quiet standing (Asai et al. 2009; Bottaro et al. 2008). Particularly, chattering-like behaviors that appear occasionally during quiet stance are the hallmark of the intermittent control (see Fig. 9 in Bottaro et al. 2005 or Fig. 3A in Asai et al. 2009, compare with Fig. 2-right of this study). In short, the intermittent control model assumes a postural-state-dependent switching between inactivation (OFF) and activation (ON) of the neural feedback controller with time-delay, which plays a critical role for stabilizing the upright posture. More specifically, the model assumes a line-shaped switching boundary passing through the origin and separating a state space of an inverted pendulum (representing the upright posture) into an OFF-region and an ON-region. The feedback controller is deactivated if the state point is in the OFF-region and, otherwise, activated in the ON-region, where appropriate actions of the switch-OFF are crucial for the stability. As shown in Fig. 9 of (Bottaro et al. 2005) and Fig. 3A of (Asai et al. 2009), typical dynamics of the intermittent control model are quite similar to the experimental postural response

shown in Fig. 2-right of this study, where both the model and experimental subjects exhibited an overdamped-system-like non-oscillatory linear trajectory toward the equilibrium posture in the very late phase of the postural recovery. This overdamped-system-like trajectory was indeed achieved by the OFF-ON chattering that takes place typically along the line-shaped switching boundary in the model (see Fig. 9 in Bottaro et al. 2005 or Fig. 3A in Asai et al. 2009). Although a choice of whether or not to switch OFF/ON the feedback control action is involuntary for the automatic postural stabilization, it is highly probable that "decision-making processes" for ON/OFF switching might generate high-beta-ERD and ERS as in decision-making processes for Go/NoGo tasks (Alegre et al. 2004; Swann et al. 2009; Zhang et al. 2008; Wu et al. 2019).

Appendix A: Model definition (Suzuki et al. 2012)

We consider a triple inverted pendulum model in the sagittal plane (Fig. A1). The upper link of the model represents the head-arm-trunk (HAT). The lower link represents the leg. The foot-link is fixed on the support surface. Masses of HAT- and leg-links are assumed to be uniformly distributed. We consider that each of ankle and hip joints can be modeled by a pin joint. The ankle and hip joint angles and body parameters are defined in Fig. A1. The equation of motions in the world coordinate system for the three links are as follows.

The HAT-link

$$m_{\mathrm{HAT}} \frac{\mathrm{d}^2}{\mathrm{dt}^2} x_{\mathrm{HAT}} = F_x$$

$$m_{\mathrm{HAT}} \frac{\mathrm{d}^2}{\mathrm{dt}^2} y_{\mathrm{HAT}} = F_y - m_{\mathrm{HAT}} g$$

$$I_{\mathrm{HAT}} \frac{\mathrm{d}^2}{\mathrm{dt}^2} (\theta_{\mathrm{a}} + \theta_{\mathrm{h}}) = (x_{\mathrm{GT}} - x_{\mathrm{HAT}}) F_y - (y_{\mathrm{GT}} - y_{\mathrm{HAT}}) F_x + \tau_{\mathrm{h}}$$

The leg-link

$$m_{\mathrm{L}} \frac{\mathrm{d}^2}{\mathrm{dt}^2} x_{\mathrm{L}} = R_x - F_x$$

$$m_{\mathrm{L}}\frac{\mathrm{d}^2}{\mathrm{dt}^2}y_{\mathrm{L}} = R_y - F_y - m_{\mathrm{L}}g$$

$$I_{\mathrm{L}}\frac{\mathrm{d}^2}{\mathrm{dt}^2}\theta_{\mathrm{a}} = (x_{\mathrm{GT}} - x_{\mathrm{L}})(-F_y) - (y_{\mathrm{GT}} - y_{\mathrm{L}})(-F_x) + (x_{\mathrm{ANK}} - x_{\mathrm{L}})R_y - (y_{\mathrm{ANK}} - y_{\mathrm{L}})R_x + \tau_{\mathrm{a}} - \tau_{\mathrm{h}}$$

The foot-link

$$m_{\mathrm{F}}\frac{\mathrm{d}^2}{\mathrm{dt}^2}x_{\mathrm{F}} = GRF_x - R_x$$

$$m_{\mathrm{F}}\frac{\mathrm{d}^2}{\mathrm{dt}^2}y_{\mathrm{F}} = GRF_y - R_y - m_{\mathrm{F}}g$$

$$I_{\mathrm{F}}\frac{\mathrm{d}^2}{\mathrm{dt}^2}\theta_{\mathrm{f}} = (x_{\mathrm{ANK}} - x_{\mathrm{F}})(-R_y) - (y_{\mathrm{ANK}} - y_{\mathrm{F}})(-R_x) + \left(x_{\mathrm{cop}}^{\mathrm{W}} - x_{\mathrm{F}}\right)GRF_y - \left(y_{\mathrm{cop}}^{\mathrm{W}} - y_{\mathrm{F}}\right)GRF_x - \tau_{\mathrm{a}}$$

In the equations of motion described above, I_{HAT}, I_{L}, and I_{F} are the inertia moment of the HAT-, the leg-, and the foot-links, respectively. F_x and F_y are the forces applied at the hip joint from the leg-link to the HAT-link. R_x and R_y are the forces applied at the ankle joint from the foot-link to the leg-link. m_{HAT}, m_{L} and m_{F} are the masses of the HAT-, leg- and foot-links. They were estimated from the total body weight of each participant using a statistical formula of m_{HAT}: m_{L}: $m_{\mathrm{F}} = 0.62: 0.35: 0.03$ (Suzuki et al. 2012). We assumed that the CoM of each link was located at the middle point of the link.

Appendix B: Inverse dynamics

We performed the inverse dynamics analysis using the model defined in Appendix A by eliminating unknown variables (F_x, F_y, R_x, R_y) from the equations of motion. Then, joint torques exerted on the ankle joint τ_{a} and hip joint τ_{h} could be estimated as

$$\tau_{\mathrm{a}} = \left(x_{\mathrm{cop}}^{\mathrm{W}} - x_{\mathrm{ANK}}\right)GRF_y - \left(y_{\mathrm{cop}}^{\mathrm{W}} - y_{\mathrm{ANK}}\right)GRF_x + (x_{\mathrm{F}} - x_{\mathrm{ANK}})(-m_{\mathrm{F}}g) - (y - y_{\mathrm{ANK}})(-m_{\mathrm{F}}a)$$

$$\tau_{\mathrm{h}} = \frac{1}{6}m_{\mathrm{L}}l_L^2\ddot{\theta}_{\mathrm{a}} - l_{\mathrm{L}}\left(\frac{m_{\mathrm{L}}}{2} + m_{\mathrm{F}}\right)(g\sin\theta_{\mathrm{a}} + a\cos\theta_{\mathrm{a}}) + l_{\mathrm{L}}\left(GRF_y\sin\theta_{\mathrm{a}} + GRF_x\cos\theta_{\mathrm{a}}\right) + \tau_{\mathrm{a}},$$

where we assumed that the foot-link is fixed on the moving support surface with no translational and

rotational movement ($\ddot{x}_{\mathrm{F}} = a,\ \ddot{y}_{\mathrm{F}} = 0,\ \ddot{\theta}_{\mathrm{f}} = 0$). Moreover, we assumed that $(x_{\mathrm{F}} - x_{\mathrm{ANK}}) = 0.02$ m, $(y_{\mathrm{F}} - y_{\mathrm{ANK}}) = -y_{\mathrm{ANK}}/2$ to compute τ_{a}.

Grants:

This study was supported by the following grants from the Ministry of Education, Culture, Sports, Science and Technology (MEXT)/Japan Society for the Promotion of Science (JSPS) KAKENHI: 20H05470 (T.N), 19H04181 (T.N), 17K13016 (Y.S), and 20K19412 (M.M).

Disclosures:

No conflicts of interest, financial or otherwise, are declared by the authors.

Author Contribution:

A.N. and T.N. conceived and designed research; A.N. and Y.S. performed experiments; A.N. analyzed data; Y.S and M.M advised on experimental and analytical methodologies; A.N. and T.N. interpreted results of experiments; A.N. prepared figures; A.N. drafted manuscript; Y.S., M.M. and T.N. edited and revised manuscript; A.N., Y.S., M.M., and T.N. approved final version of manuscript.

References

Adkin AL, **Campbell AD**, **Chua R**, **Carpenter MG**. The influence of postural threat on the cortical response to unpredictable and predictable postural perturbations. *Neurosci Lett* 435: 120–125, 2008.

Adkin AL, **Quant S**, **Maki BE**, **McIlroy WE**. Cortical responses associated with predictable and unpredictable compensatory balance reactions. *Exp Brain Res* 172: 85, 2006.

Alegre M, **Gurtubay IG**, **Labarga A**, **Iriarte J**, **Valencia M**, **Artieda J**. Frontal and central oscillatory changes related to different aspects of the motor process: a study in go/no-go paradigms. *Exp Brain Res* 159: 14–22, 2004.

Androulidakis AG, **Doyle LMF**, **Gilbertson TP**, **Brown P**. Corrective movements in response to displacements in visual feedback are more effective during periods of 13–35 Hz oscillatory synchrony

in the human corticospinal system. *Eur J Neurosci* 24: 3299–3304, 2006.

Asai Y, **Tasaka Y**, **Nomura K**, **Nomura T**, **Casadio M**, **Morasso P**. A Model of Postural Control in Quiet Standing: Robust Compensation of Delay-Induced Instability Using Intermittent Activation of Feedback Control. *PLOS ONE* 4: e6169, 2009.

Bigdely-Shamlo N, **Mullen T**, **Kothe C**, **Su K-M**, **Robbins KA**. The PREP pipeline: standardized preprocessing for large-scale EEG analysis. *Front Neuroinformatics* 9, 2015.

Bolton DAE. The role of the cerebral cortex in postural responses to externally induced perturbations. *Neurosci Biobehav Rev* 57: 142–155, 2015.

Bottaro A, **Casadio M**, **Morasso PG**, **Sanguineti V**. Body sway during quiet standing: Is it the residual chattering of an intermittent stabilization process? *Hum Mov Sci* 24: 588–615, 2005.

Bottaro A, **Yasutake Y**, **Nomura T**, **Casadio M**, **Morasso P**. Bounded stability of the quiet standing posture: An intermittent control model. *Hum Mov Sci* 27: 473–495, 2008.

Bruijn SM, **Van Dieën JH**, **Daffertshofer A**. Beta activity in the premotor cortex is increased during stabilized as compared to normal walking. *Front Hum Neurosci* 9, 2015.

Buzsáki G, **Anastassiou CA**, **Koch C**. The origin of extracellular fields and currents — EEG, ECoG, LFP and spikes. *Nat Rev Neurosci* 13: 407–420, 2012.

Cassim F, **Monaca C**, **Szurhaj W**, **Bourriez J-L**, **Defebvre L**, **Derambure P**, **Guieu J-D**. Does post-movement beta synchronization reflect an idling motor cortex? *Neuroreport* 12: 3859–3863, 2001.

Chatrian GE, **Lettich E**, **Nelson PL**. Ten Percent Electrode System for Topographic Studies of Spontaneous and Evoked EEG Activities. *Am J EEG Technol* 25: 83–92, 1985.

Collins JJ, **De Luca CJ**. Random Walking during Quiet Standing. *Phys Rev Lett* 73: 764–767, 1994.

Davis H, **Davis PA**, **Loomis AL**, **Harvey EN**, **Hobart G**. Electrical reactions of the human brain to auditory stimulation during sleep. *J Neurophysiol* 2: 500–514, 1939.

Delorme A, **Makeig S**. EEGLAB: an open source toolbox for analysis of single-trial EEG dynamics including independent component analysis. *J Neurosci Methods* 134: 9–21, 2004.

Dietz V, **Quintern J**, **Berger W**. Cerebral evoked potentials associated with the compensatory reactions following stance and gait perturbation. *Neurosci Lett* 50: 181–186, 1984.

Dietz V, **Quintern J**, **Berger W**, **Schenck E**. Cerebral potentials and leg muscle e.m.g. responses associated with stance perturbation. *Exp Brain Res* 57: 348–354, 1985.

Dimitrov B, **Gavrilenko T**, **Gatev P**. Mechanically evoked cerebral potentials to sudden ankle dorsiflexion in human subjects during standing. *Neurosci Lett* 208: 199–202, 1996.

Dunnett CW. A Multiple Comparison Procedure for Comparing Several Treatments with a Control. *J Am Stat Assoc* 50: 1096–1121, 1955.

Dunnett CW. New Tables for Multiple Comparisons with a Control. *Biometrics* 20: 482, 1964.

Engel AK, **Fries P**. Beta-band oscillations—signalling the status quo? *Curr Opin Neurobiol* 20: 156–165, 2010.

Ferree TC, **Luu P**, **Russell GS**, **Tucker DM**. Scalp electrode impedance, infection risk, and EEG data quality. *Clin Neurophysiol* 112: 536–544, 2001.

Frzovic D, **Morris ME**, **Vowels L**. Clinical tests of standing balance: Performance of persons with multiple sclerosis. *Arch Phys Med Rehabil* 81: 215–221, 2000.

Geurts ACH, **de Haart M**, **van Nes IJW**, **Duysens J**. A review of standing balance recovery from stroke. *Gait Posture* 22: 267–281, 2005.

Gilbertson T, **Lalo E**, **Doyle L**, **Lazzaro VD**, **Cioni B**, **Brown P**. Existing Motor State Is Favored at the Expense of New Movement during 13-35 Hz Oscillatory Synchrony in the Human Corticospinal System. *J Neurosci* 25: 7771–7779, 2005.

Heinrichs-Graham E, **Wilson TW**. Is an absolute level of cortical beta suppression required for proper movement? Magnetoencephalographic evidence from healthy aging. *NeuroImage* 134: 514–521, 2016.

Horak FB, **Nashner LM**. Central programming of postural movements: adaptation to altered support-surface configurations. *J Neurophysiol* 55: 1369–1381, 1986.

Horak FB, **Nutt JG**, **Nashner LM**. Postural inflexibility in parkinsonian subjects. *J Neurol Sci* 111: 46–58, 1992.

Jacobs JV, **Horak FB**. Cortical control of postural responses. *J Neural Transm* 114: 1339, 2007.

Jurcak V, **Tsuzuki D**, **Dan I**. 10/20, 10/10, and 10/5 systems revisited: Their validity as relative head-surface-based positioning systems. *NeuroImage* 34: 1600–1611, 2007.

Jurkiewicz MT, **Gaetz WC**, **Bostan AC**, **Cheyne D**. Post-movement beta rebound is generated in motor cortex: Evidence from neuromagnetic recordings. *NeuroImage* 32: 1281–1289, 2006.

Lalo E, **Thobois S**, **Sharott A**, **Polo G**, **Mertens P**, **Pogosyan A**, **Brown P**. Patterns of Bidirectional Communication between Cortex and Basal Ganglia during Movement in Patients with Parkinson Disease. *J Neurosci* 28: 3008–3016, 2008.

Lilliefors HW. On the Kolmogorov-Smirnov Test for Normality with Mean and Variance Unknown. *J Am Stat Assoc* 62: 399–402, 1967.

Loo SK, **Miyakoshi M**, **Tung K**, **Lloyd E**, **Salgari G**, **Dillon A**, **Chang S**, **Piacentini J**, **Makeig S**. Neural activation and connectivity during cued eye blinks in Chronic Tic Disorders. *NeuroImage Clin* 24: 101956, 2019.

Makeig S. Auditory event-related dynamics of the EEG spectrum and effects of exposure to tones. *Electroencephalogr Clin Neurophysiol* 86: 283–293, 1993.

Matsuda K, **Suzuki Y**, **Yoshikawa N**, **Yamamoto T**, **Kiyono K**, **Tanahashi T**, **Endo T**, **Fukada K**, **Nomura K**, **Sakoda S**, **Nomura T**. Postural flexibility during quiet standing in healthy elderly and patients with Parkinson's disease. In: *2016 38th Annual International Conference of the IEEE Engineering in Medicine and Biology Society (EMBC)*. 2016 38th Annual International Conference of the IEEE Engineering in Medicine and Biology Society (EMBC). 2016, p. 29–32.

Merletti R, **Di Torino P**. Standards for Reporting EMG Data. *J Electromyogr Kinesiol* 9: 4, 1999.

Mierau A, **Pester B**, **Hülsdünker T**, **Schiecke K**, **Strüder HK**, **Witte H**. Cortical Correlates of Human Balance Control. *Brain Topogr* 30: 434–446, 2017.

Mochizuki G, **Sibley KM**, **Cheung HJ**, **Camilleri JM**, **McIlroy WE**. Generalizability of perturbation-evoked cortical potentials: Independence from sensory, motor and overall postural state. *Neurosci Lett* 451: 40–44, 2009.

Mullen TR, **Kothe CAE**, **Chi YM**, **Ojeda A**, **Kerth T**, **Makeig S**, **Jung T**, **Cauwenberghs G**. Real-time neuroimaging and cognitive monitoring using wearable dry EEG. *IEEE Trans Biomed Eng* 62: 2553–2567, 2015.

Muthukumaraswamy SD. The use of magnetoencephalography in the study of psychopharmacology (pharmaco-MEG). *J Psychopharmacol (Oxf)* 28: 815–829, 2014.

Neuper C, **Pfurtscheller G**. Post-movement synchronization of beta rhythms in the EEG over the cortical foot area in man. *Neurosci Lett* 216: 17–20, 1996.

Nomura T, **Oshikawa S**, **Suzuki Y**, **Kiyono K**, **Morasso P**. Modeling human postural sway using an intermittent control and hemodynamic perturbations. *Math Biosci* 245: 86–95, 2013.

Pastötter B, **Hanslmayr S**, **Bäuml K-H**. Inhibition of Return Arises from Inhibition of Response Processes: An Analysis of Oscillatory Beta Activity. *J Cogn Neurosci* 20: 65–75, 2008.

Payne A, Ting L. Cortical Responses to Balance Perturbation are Abnormal in Parkinson's Disease (4129). *Neurology* 94: 4129, 2020.

Payne AM, Hajcak G, Ting LH. Dissociation of muscle and cortical response scaling to balance perturbation acceleration. *J Neurophysiol* 121: 867–880, 2018.

Payne AM, Ting LH, Hajcak G. Do sensorimotor perturbations to standing balance elicit an error-related negativity? *Psychophysiology* 56: e13359, 2019.

Perera T, Tan JL, Cole MH, Yohanandan SAC, Silberstein P, Cook R, Peppard R, Aziz T, Coyne T, Brown P, Silburn PA, Thevathasan W. Balance control systems in Parkinson's disease and the impact of pedunculopontine area stimulation. *Brain* 141: 3009–3022, 2018.

Peterson SM, **Ferris DP**. Differentiation in Theta and Beta Electrocortical Activity between Visual and Physical Perturbations to Walking and Standing Balance. *eNeuro* 5, 2018.

Pfurtscheller G, **Lopes da Silva FH**. Event-related EEG/MEG synchronization and desynchronization: basic principles. *Clin Neurophysiol* 110: 1842–1857, 1999.

Pfurtscheller G, **Stancák A**, **Neuper C**. Post-movement beta synchronization. A correlate of an idling motor area? *Electroencephalogr Clin Neurophysiol* 98: 281–293, 1996.

Quant S, **Adkin AL**, **Staines WR**, **Maki BE**, **McIlroy WE**. The effect of a concurrent cognitive task on cortical potentials evoked by unpredictable balance perturbations. *BMC Neurosci* 5: 18, 2004.

Quant S, **Maki BE**, **McIlroy WE**. The association between later cortical potentials and later phases of postural reactions evoked by perturbations to upright stance. *Neurosci Lett* 381: 269–274, 2005.

Rossiter HE, **Davis EM**, **Clark EV**, **Boudrias M-H**, **Ward NS**. Beta oscillations reflect changes in motor cortex inhibition in healthy ageing. *NeuroImage* 91: 360–365, 2014.

Slobounov S, **Hallett M**, **Stanhope S**, **Shibasaki H**. Role of cerebral cortex in human postural control: an EEG study. *Clin Neurophysiol* 116: 315–323, 2005.

Solis-Escalante T, **van der Cruijsen J**, **de Kam D**, **van Kordelaar J**, **Weerdesteyn V**, **Schouten AC**. Cortical dynamics during preparation and execution of reactive balance responses with distinct postural demands. *NeuroImage* 188: 557–571, 2019.

Solopova IA, **Kazennikov OV**, **Deniskina NB**, **Levik YS**, **Ivanenko YP**. Postural instability enhances motor responses to transcranial magnetic stimulation in humans. *Neurosci Lett* 337: 25–28, 2003.

Staines RW, **McIlroy WE**, **Brooke JD**. Cortical representation of whole-body movement is modulated by proprioceptive discharge in humans. *Exp Brain Res* 138: 235–242, 2001.

Suzuki Y, **Nomura T**, **Casadio M**, **Morasso P**. Intermittent control with ankle, hip, and mixed strategies during quiet standing: A theoretical proposal based on a double inverted pendulum model. *J Theor Biol* 310: 55–79, 2012.

Swann N, **Tandon N**, **Canolty R**, **Ellmore TM**, **McEvoy LK**, **Dreyer S**, **DiSano M**, **Aron AR**. Intracranial EEG Reveals a Time- and Frequency-Specific Role for the Right Inferior Frontal Gyrus and Primary Motor Cortex in Stopping Initiated Responses. *J Neurosci* 29: 12675–12685, 2009.

Todd NPM, **McLean A**, **Paillard A**, **Kluk K**, **Colebatch JG**. Vestibular evoked potentials (VsEPs) of cortical origin produced by impulsive acceleration applied at the nasion. *Exp Brain Res* 232: 3771–3784, 2014.

Varghese JP, **Beyer KB**, **Williams L**, **Miyasike-daSilva V**, **McIlroy WE**. Standing still: Is there a role for the cortex? *Neurosci Lett* 590: 18–23, 2015.

Varghese JP, **Marlin A**, **B. Beyer K**, **Staines WR**, **Mochizuki G**, **McIlroy WE**. Frequency characteristics of cortical activity associated with perturbations to upright stability. *Neurosci Lett* 578: 33–38, 2014.

Varghese JP, **McIlroy RE**, **Barnett-Cowan M**. Perturbation-evoked potentials: Significance and application in balance control research. *Neurosci Biobehav Rev* 83: 267–280, 2017.

Vinding MC, **Tsitsi P**, **Piitulainen H**, **Waldthaler J**, **Jousmäki V**, **Ingvar M**, **Svenningsson P**, **Lundqvist D**. Attenuated beta rebound to proprioceptive afferent feedback in Parkinson's disease. *Sci Rep* 9: 2604, 2019.

Visser JE, **Carpenter MG**, **van der Kooij H**, **Bloem BR**. The clinical utility of posturography. *Clin Neurophysiol* 119: 2424–2436, 2008.

van Wijk BCM, **Daffertshofer A**, **Roach N**, **Praamstra P**. A Role of Beta Oscillatory Synchrony in Biasing Response Competition? *Cereb Cortex* 19: 1294–1302, 2009.

Winkler I, **Debener S**, **Müller K**, **Tangermann M**. On the influence of high-pass filtering on ICA-

based artifact reduction in EEG-ERP. In: *2015 37th Annual International Conference of the IEEE Engineering in Medicine and Biology Society (EMBC)*. 2015 37th Annual International Conference of the IEEE Engineering in Medicine and Biology Society (EMBC). 2015, p. 4101–4105.

Winter DA, **Rau G**, **Kadefors R**, **Broman H**, **De Luca C**. Units, Terms and Standards in the Reporting of EMG Research.pdf [Online]. *Rep Ad Hoc Comm Int Soc Electrophysiol Kinesiol* , 1980http://www.bu.edu/nmrc/files/2013/12/B-4.pdf [23 Sep. 2019].

Wittenberg E, **Thompson J**, **Nam CS**, **Franz JR**. Neuroimaging of Human Balance Control: A Systematic Review. *Front Hum Neurosci* 11, 2017.

Woollacott M, **Shumway-Cook A**. Attention and the control of posture and gait: a review of an emerging area of research. *Gait Posture* 16: 1–14, 2002.

Wu H-M, **Hsiao F-J**, **Chen R-S**, **Shan D-E**, **Hsu W-Y**, **Chiang M-C**, **Lin Y-Y**. Attenuated NoGo-related beta desynchronisation and synchronisation in Parkinson's disease revealed by magnetoencephalographic recording. *Sci Rep* 9: 7235, 2019.

Yamamoto T, **Smith CE**, **Suzuki Y**, **Kiyono K**, **Tanahashi T**, **Sakoda S**, **Morasso P**, **Nomura T**. Universal and individual characteristics of postural sway during quiet standing in healthy young adults. *Physiol Rep* 3: e12329, 2015.

Yamamoto T, **Suzuki Y**, **Nomura K**, **Nomura T**, **Tanahashi T**, **Fukada K**, **Endo T**, **Sakoda S**. A Classification of Postural Sway Patterns During Upright Stance in Healthy Adults and Patients with Parkinson's Disease. *J Adv Comput Intell Intell Inform* 15: 997–1010, 2011.

Yoshida T, **Masani K**, **Zabjek K**, **Chen R**, **Popovic MR**. Dynamic Increase in Corticomuscular Coherence during Bilateral, Cyclical Ankle Movements. *Front Hum Neurosci* 11, 2017.

Zhang Y, **Chen Y**, **Bressler SL**, **Ding M**. Response preparation and inhibition: The role of the cortical sensorimotor beta rhythm. *Neuroscience* 156: 238–246, 2008.

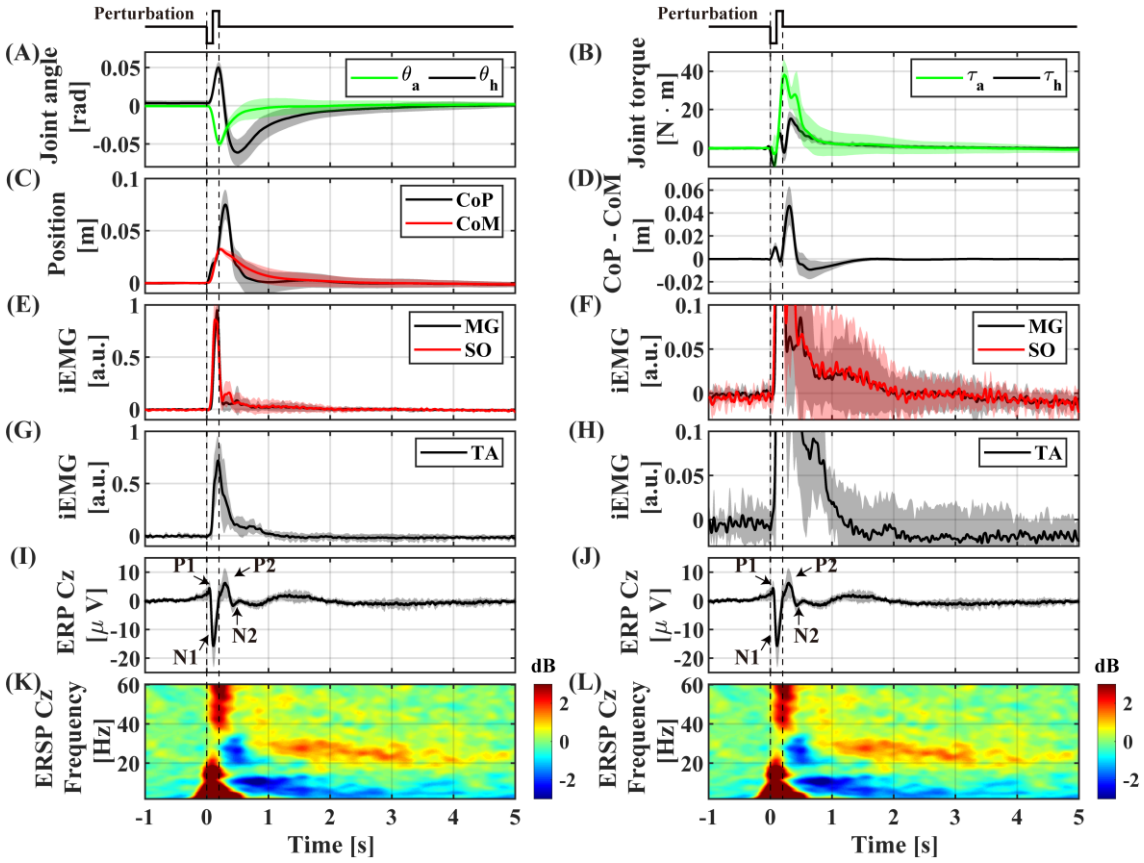

Figure 1. Event-locked average profiles (averaged across participants) triggered by the perturbation-onset. (A) ankle and hip joint angles, (B) joint torques obtained by the inverse dynamics analysis, (C) CoP and CoM positions, (E) normalized iEMGs of Medial-Gastrocnemius and Soleus, (F) magnification of (E), (G) normalized iEMG of Tibialis Anterior, (H) magnification of (G), (I) ERP of Cz-electrode, (J) the same as (I), (K) ERSP of Cz electrode, (L) the same as (K). The light color shaded area in each of (A)-(J) is the standard deviation, representing the distribution across participants.

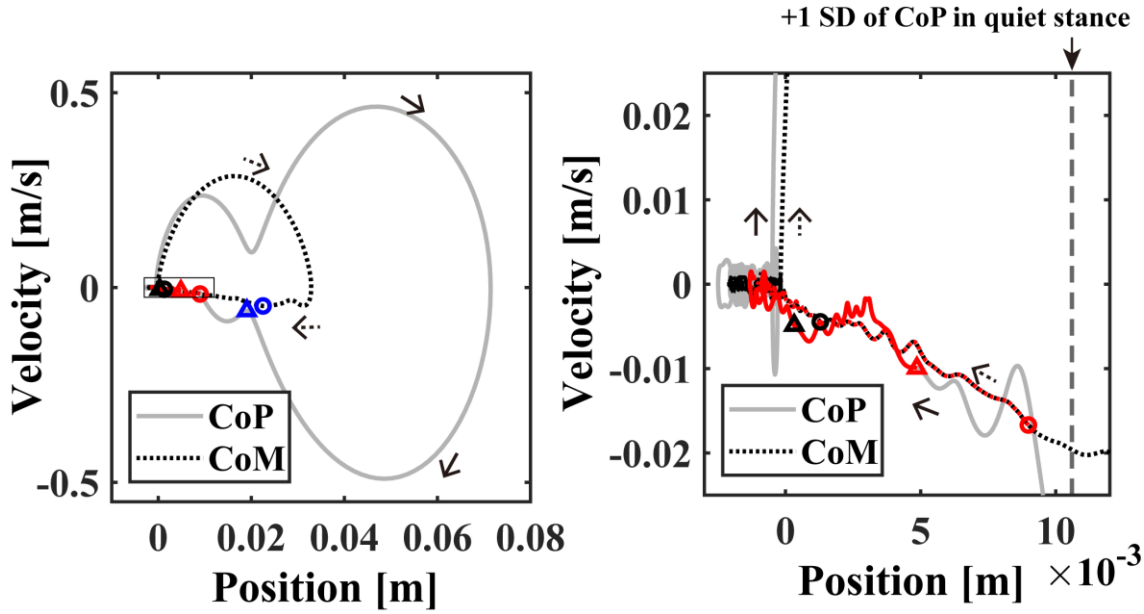

Figure 2. The event-locked average of CoP/CoM profile (averaged across subjects) in the CoP/CoM-position v.s. the CoP/CoM-velocity phase plane for $t \in [-3, 8]$ s. The small blue, red and black circles plotted on the CoM (solid-gray) trajectories in the left and/or right panels indicate the time instants of 0.5, 1.0 and 2.0 s, respectively. The triangles with the same colors indicate the corresponding time instants on the CoP (dotted) trajectories. The right panel is an enlargement of the rectangular region near the origin in the left panel. The time-duration with beta rebound (ERS) about $t \in [1.0, 4.0]$ s with significantly large power was indicated by the red trajectories. The vertical dashed line in the right panel indicates the standard deviation of the postural sway during the quiet standing.

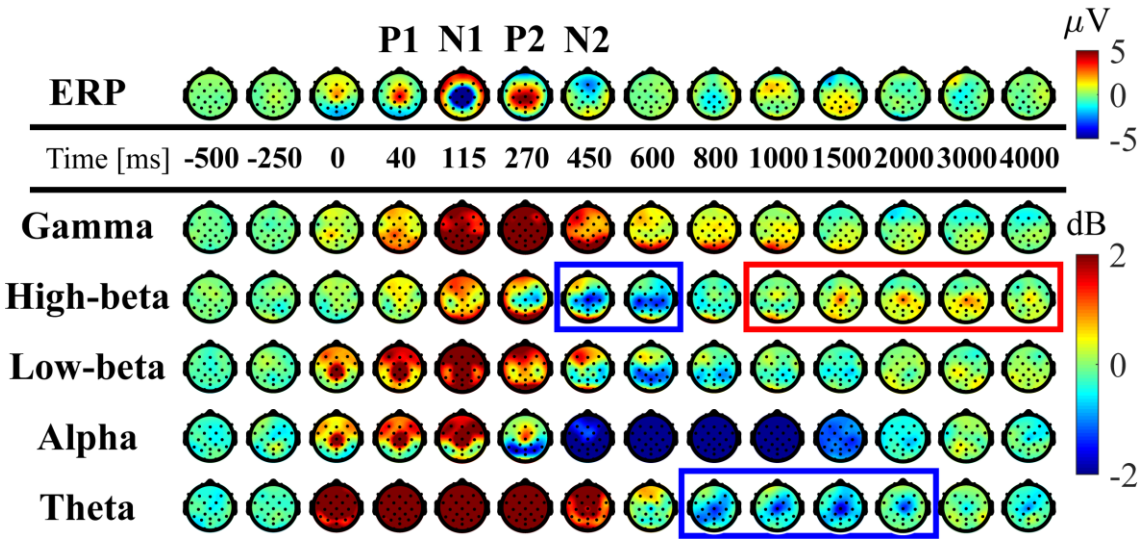

Figure 3. Spatial distributions of ERP and ERSP on the scalp (averaged across participants). Upper panel: time-changes in the spatial distribution of the potential on the scalp. Lower panels: time-changes in the spatial distribution of EEG-power, i.e., ERSP, for the frequency-bands of theta (3-7 Hz), alpha (8-13 Hz), low-beta (13-20 Hz), high-beta (20-30 Hz), gamma (40-60 Hz) plotted on the scalp. The scalps surrounded by the red and blue rectangulars indicate that the amplitude was significantly larger (ERS) and smaller (ERD) than the mean power prior to the perturbation.

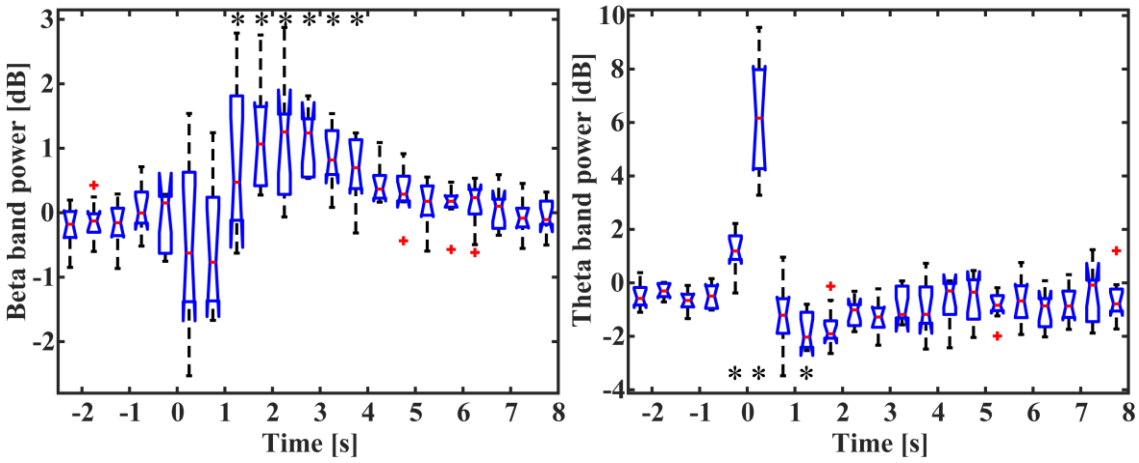

Figure 4. Time-changes in the average powers of high-beta-band (left) and theta-band. t = 0 corresponds to the perturbation-onset. Average power values were calculated for each participant from -2.5 s to 8 s for every 0.5 s interval representing each box of the plots. The powers of the boxes with the symbol * were significantly larger and smaller than the resting potential ($p < 0.05$, Dunnett's test), respectively, for the high-beta and theta bands.

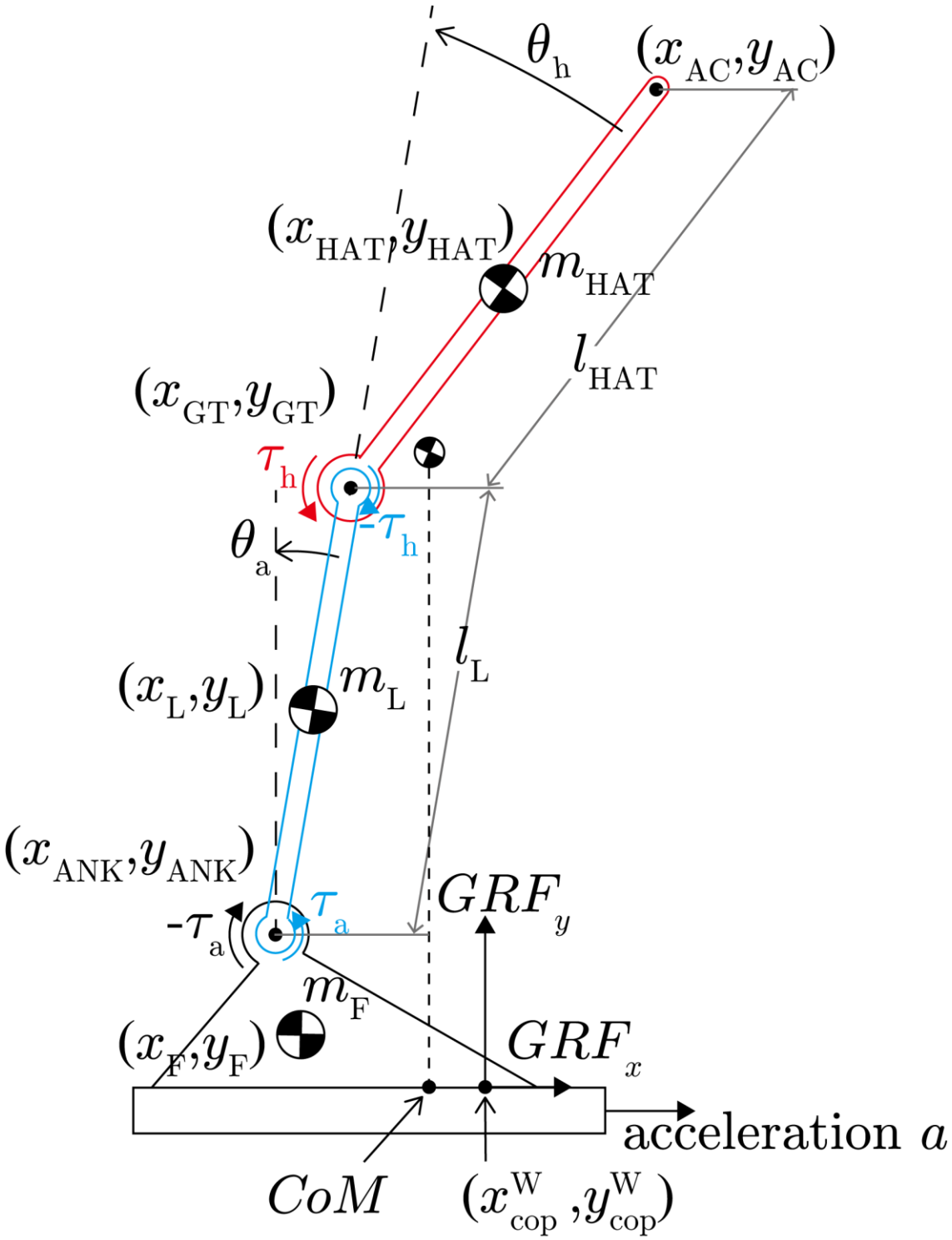

Figure A1. A triple inverted pendulum with a foot-link fixed on the support-surface. The model consists of links of HAT, leg and foot with a pin joint at the ankle and hip. See text of the Appendix.